

CHEMISTRY AND MINERALOGY OF EARTH'S MANTLE

Ca-Al-silicate inclusions in natural moissanite (SiC)

SIMONPIETRO DI PIERRO^{1,*} AND EDWIN GNOS²¹UMR CNRS 5570, Laboratoire de Sciences de la Terre, ENS Lyon, France²Natural History Museum of Geneva, route de Malagnou 1, CP 6434, 1211 Geneve 6, Switzerland

ABSTRACT

Hundred-micrometer-sized calcium-aluminum-silicates (CAS) inclusions occur in moissanite-4H, moissanite-15R, and moissanite-6H from Turkey. These inclusions commonly consist of tabular exsolution lamellae of two different minerals. By combined electron microprobe and Raman spectroscopy analysis, at least eight different, essentially Mg- and Fe-free Ca-Al-silicate or Al-silicate phases have been discerned. The most common phase is dmisteinbergite, a hexagonal modification of $\text{CaAl}_2\text{Si}_2\text{O}_8$, occurring in association with lamellae of $\text{Ca}_x(\text{Al,Si})_{1-x}\text{O}_3$ or $\text{Ca}_{1-x}(\text{Al,Si})_{2+x}\text{O}_5$ compositions. All three phases contain significant amounts of BaO (up to 2 mol% of celsian component in dmisteinbergite), SrO, SO_3 , and light rare earth elements (LREE). In particular, $\text{Ca}_{1-x}(\text{Al,Si})_{2+x}\text{O}_5$ contains up to 2.1 wt% of LREE, 3.9 wt% of F, and significant traces of Cl, while it is also associated to osbornite (TiN). Pure ghelenite, $\text{Ca}_2\text{Al}_2\text{SiO}_7$, and three additional compositions, namely $\text{CaAl}_{4-x}\text{Si}_x\text{O}_7$, $\text{Ca}_{1-x}(\text{Al,Si})_{3+x}\text{O}_6$, and $\text{Ca}_{3-x}(\text{Al,Si})_{6+x}\text{O}_{14}$ have been found, either occurring as single grains or forming exsolution lamellae. They also contain significant amounts of BaO, SrO, SO_3 , and LREE. One last intriguing phase is composed in average of 65.9 wt% SiO_2 , 17.4% Al_2O_3 , 3.0% alkalis, 6.0% BaO, 2.0% $\text{CaO}+\text{MgO}$, 0.9% ZrO_2 , and up to 0.5% LREE. Dmisteinbergite and ghelenite show Raman peaks in very good agreement with literature data, $\text{Ca}_x(\text{Al,Si})_{1-x}\text{O}_3$ shows main Raman modes at 416 and 1009 cm^{-1} , $\text{Ca}_{1-x}(\text{Al,Si})_{3+x}\text{O}_6$ at 531 and 1579 cm^{-1} while $\text{Ca}_{3-x}(\text{Al,Si})_{6+x}\text{O}_{14}$ has a strong peak at 553 cm^{-1} . $\text{CaAl}_{4-x}\text{Si}_x\text{O}_7$ shows a weak Raman pattern, while $\text{Ca}_{1-x}(\text{Al,Si})_{2+x}\text{O}_5$ has no detectable Raman modes. Since the association moissanite-CAS is thermodynamically not stable at ambient pressure and moissanite crystals hosting the CAS phases have $\delta^{13}\text{C}$ values typical of deep-mantle origin, we interpret the CAS inclusions as partially retrogressed HP minerals. Striking analogies exist between observed CAS compositions and experimentally obtained HP-HT mineralogy. For instance, $\text{Ca}_x(\text{Al,Si})_{1-x}\text{O}_3$ contains up to 25 mol% of Al_2O_3 , which is considered as the upper limit of alumina solubility in Ca-perovskite. The study confirms that CAS phases are an important mantle depository for large ion lithophile elements (LILE) and LREE.

Keywords: Moissanite, dmisteinbergite, ghelenite, unknown CAS mineral, Raman spectra, mineral composition

INTRODUCTION

The natural occurrence of moissanite, natural α -silicon carbide, under terrestrial conditions was vigorously debated until the end of the 1980s. Milton and Vitaliano (1984) critically but correctly proposed a series of six independent criteria to discern natural moissanite occurrences from synthetic SiC contaminations. Extensive field researches in the last three decades fulfilled most of these criteria. The first one concerned the *finding of moissanite as inclusion in other minerals*. In fact, moissanite crystals were reported included in diamonds and carbonados from kimberlites and lamproites from many continental cratons in Russia (Yakutia; Marshintsev 1990), China (Fuxian; Leung 1990), U.S.A. (Colorado; McCammon et al. 1997; Otter and Gurney 1986, 1989), South Africa (Monastery Mine; Moore et al. 1986; Moore and Gurney 1989; Koffiefontein mine, Klein-BenDavid et al. 2007), Central Africa (De et al. 1998), Australia (Argyle lamproite; Jaques et al. 1989), and Brazil (Sao

Luis River placers; Wilding et al. 1991; Svisero 1995; De et al. 1998; Kaminsky 2012). Moissanite was also reported included in garnets from a Chinese retrogressive eclogite (Qi et al. 2007). These authors show excellent thin section microphotographs of a dozen of moissanite crystals included, along with coesite and rutile, in pyrope. In serpentinite from the Chinese Dabie Mountains, Xu et al. (2008) present thin section microphotographs of moissanite associated to rutile and baddeleyite. Moreover, moissanite was also reported as inclusions in olivine from the diamondiferous Karashoho pipe from the Bukantau mountains from Uzbekistan (Golovko and Kaminsky 2010), and in garnets from felsic granulites from the Moldanubian Zone of the Bohemian Massif (Perraki and Faryad 2014). These latter authors also show thin section microphotographs where moissanite is unequivocally contained within the hosting mineral. Finally, from the Luobusa ophiolite, Tibet, Robinson et al. (2015) and Liang et al. (2014) reported moissanite in olivine from peridotite, and in Cr-spinel from dunite, respectively. *Euhedral, unbroken crystals*, the second criterion, have been reported from Fuxian (Leung et al. 1990; Leung 1990), Turkey (Di Pierro et al. 2003), and Yakutia (Shiryaev et al. 2011), while abundant silicon and

* E-mail: simonpietro.dipierro@saint-gobain.com

Special collection information can be found at <http://www.minsocam.org/MSA/AmMin/special-collections.html>.

Fe-silicides, systematically reported as inclusions in terrestrial moissanite and considered to represent former *melt-inclusions* (Marschintsev 1990; Pankov and Spetsius 1990; Mathez et al. 1995; Bai et al. 1993, 2000, 2003; Di Pierro et al. 2003; Robinson et al. 2004), is the third criterion to distinguish synthetic from natural moissanite. Besides the above-mentioned Chinese findings, *freshly broken rocks showing abundant enclosed SiC*, the fourth criterion, have been reported by Bauer et al. (1963), Leung (1988), and Di Pierro et al. (2003). The fifth criterion proposed by Milton and Vitaliano (1984) is to find *moissanite in eutectic or sutured intergrowth with magmatic minerals*. Mathez et al. (1995) reported three oxygen-bearing inclusions in natural SiC from Yakutia, namely one FeMg-silicate grain directly associated to moissanite, a sinoite grain, $\text{Si}_2\text{N}_2\text{O}$, and a crystal of a light rare earth element (LREE) silicate containing 75 wt% of LREE_2O_3 , both associated to silicide inclusions in SiC. Leung et al. (1996) reported rutile grains included in moissanite in kimberlite at Kimberley. Oleynikov et al. (1987) reported Al-silicate included in moissanite from mafic rocks from Russia. Robinson et al. (2004) reported gehlenite-like composition from a grain included in moissanite from Luobusa, while Gao and Liu (2008) found zircon included in moissanite from a carbonatite xenolith. At the best of our knowledge no association of SiC and oxides has been reported in synthetic SiC literature. The sixth, arguable, criterion of Milton and Vitaliano (1984) of finding *large (over 1 cm) crystal* has not been fulfilled so far.

By analogy with similar findings from kimberlitic (Pankov and Spetsius 1990; Leung et al. 1990; Mathez et al. 1995; Shiryayev et al. 2011) and ophiolitic environments (Bai et al. 2000; Robinson et al. 2004; Trumbull et al. 2009; Yang et al. 2011), a natural origin of the Turkish moissanite was proposed, mainly based on presence of silicon and Fe-silicide inclusions (Di Pierro et al. 2003). A subsequent carbon isotope study confirmed that the moissanites have $\delta^{13}\text{C}$ values typical of other occurrences from the deep mantle (Trumbull et al. 2009).

Here we report the discovery of eight different LREE- and Ba-bearing Ca-Al-silicates (CAS) and Al-silicates (AS), found as hundred-micrometer-grain-sized inclusions in moissanite from Turkey (Di Pierro et al. 2003). We will show that from a thermodynamic point of view the observed Ca-Al mineral association can be neither stable under ambient-pressure conditions of the Acheson process nor any other industrial way of producing silicon-carbide (Knippenberg 1963; Gauthier 1978; Jepps and Page 1983; Lindstad 2002). Zhou and Telle (2010), in fact, using FactSage software package found that undesired Al_2O_3 , CaO , Fe_2O_3 , and MgO impurities from the Acheson raw materials, can condense as anorthite, gehlenite, krotite, CaAl_2O_4 , wollastonite, and mullite, in areas at temperatures below 1500 °C during the run, while in the internal and hotter part of the Acheson reactor above 1900 °C, where α -SiC modifications are stable, elementary Al, Ca, Fe, and Mg are present in the gas form.

SAMPLES AND METHODS

As described in Di Pierro et al. (2003), the here-reported rock is one unique specimen found at beach by Salvatore Musacchia, around 150 km NW from Izmir, Turkey. The source outcrop having not been found so far, the sample is thought to be derived from Tertiary volcanic rocks outcropping in the area (e.g., Innocenti et al. 2005; Aldanmaz et al. 2006). The sample shows a bulk bluish color and consists of a very fine-grained mixture of brucite, phlogopite, calcite, and magnesite, in

which abundant macrocrysts of quartz and moissanite occur.

Besides optical microscopy, electron microprobe analyses (EMPA) have been performed at the Institute for Geology, University of Bern using a Cameca SX 50 microprobe, wavelength-dispersive spectrometers (WDS), and operating conditions of 15 kV and 20 nA. Natural and synthetic silicate and oxide standard were used: almandine (Fe), olivine (Mg), orthoclase (K, Si), anorthite (Ca, Al), eskolaite (Cr), tephroite (Mn), albite (Na), ilmenite (Ti), and bunsenite (Ni). Detection limits in element wt% are Si 0.02; Ti 0.03; Zr 0.04; Na 0.03; Al 0.02; Y 0.06; Ce 0.08; La 0.08; Fe 0.07; Mn 0.08; Mg 0.03; Ca 0.02; Sr 0.07; Ba 0.08; K 0.02; Na 0.03; S 0.03; and F 0.13 and Cl 0.04. Additional analyses were obtained at the University Claude Bernard Lyon-1 and Ecole Normale Supérieure (ENS) of Lyon (Joint Laboratory of Earth Sciences), operating conditions of 15 kV and 20 nA.

Raman spectra were recorded with a DILOR XY spectrometer equipped with confocal optics and a nitrogen-cooled CCD detector, at the ENS-Lyon. A microscope has been used to focus the excitation laser beam (514 nm lines of a Spectra Physics Ar+ laser) to a 2 μm spot and to collect the Raman signal in the backscattered direction. Collecting times were 20 to 60 s at low power of 2–30 mW, to avoid sample deterioration (not observed during spectra acquisition).

X-ray mapping was performed with a energy-dispersive system (EDS) on a Jeol 7600F scanning electron microscope (SEM) using an acceleration voltage of 15 keV conditions, at Saint-Gobain Recherche.

CHARACTERIZATION OF CAS PHASES

In a polished thin section containing 341 moissanite crystals, CAS inclusions have been observed in at least 21 grains (~6%). Hosting silicon-carbide crystals are 6H, 15R, or 4H polytypes.

Ca-Al-silicates and Al-silicates are coarse-grained, up to 150 μm in length, tabular or xenomorphic, or drop-like in shape (Figs. 1–3) and found as inclusions or in oriented contact with moissanite crystals.

In reflected light and in BSE images, CAS and AS phases show different shades of gray while they normally show either

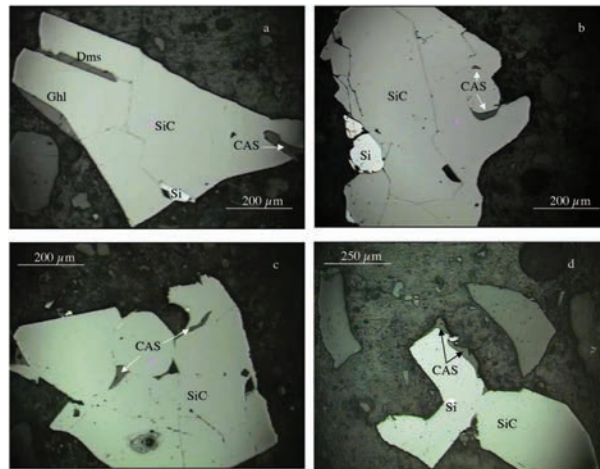


FIGURE 1. Thin section photos (reflected light) of Ca-Al-silicates (CAS) in contact or forming inclusions in moissanite crystals. (a) SiC no. 78: system of multiple inclusions. CAS are in gray, metallic Si in white. The gray crystal growing on the left rim is gehlenite (Ghl: analyses 21–24 in Table 1). The crystal above is Dmisteinbergite (Dms: analysis 17 in Table 1). The CAS crystal to the right has $\text{Ca}_{1-x}(\text{Al,Si})_{3+x}\text{O}_6$ composition. (b) SiC no. 199: the two gray inclusions of CAS are arrowed. Details of the larger CAS inclusion, along with the EDS X-ray mapping, are presented in Figure 2. (c) SiC no. 85 containing two gray inclusions of CAS. (d) SiC no. 244 with a CAS crystal (arrowed: analyses 2–4, and 10–11 in Table 1) on the surface, and associated with a TiN grain, in white. Details of this grain, along with the EDS X-ray mapping, are presented in Figure 3. (Color online.)

very low or no birefringence (Fig. 1). They are mainly included in moissanite crystals, but some are growing on SiC boundaries (Fig. 1). They occur also associated to silicon and Fe-Ti-Al-Ca-silicite inclusions in moissanite (Fig. 1). Most CAS inclusions present exsolution textures, consisting of 10–20 μm wide and maximally 50 μm long dark and bright lamellae, intersecting at low angles (Figs. 2–3). Point counting shows that the two exsolved phases

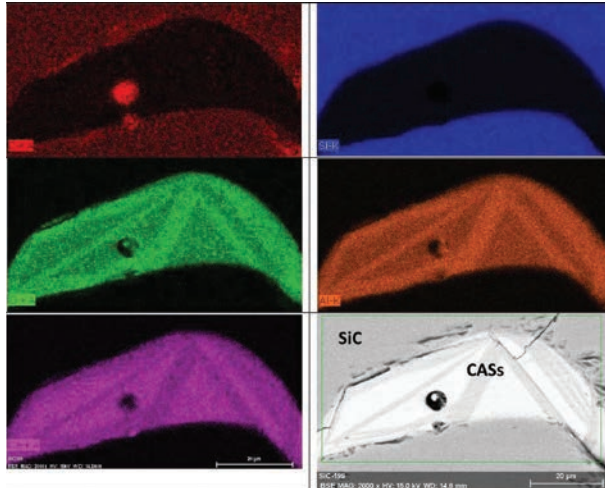


FIGURE 2. X-ray mapping of CAS inclusion in SiC no. 199. Dark lamellae in the BSE image are dmisteinbergite, while bright areas have a $\text{Ca}_x(\text{Al},\text{Si})_{1-x}\text{O}_3$ composition. (Color online.)

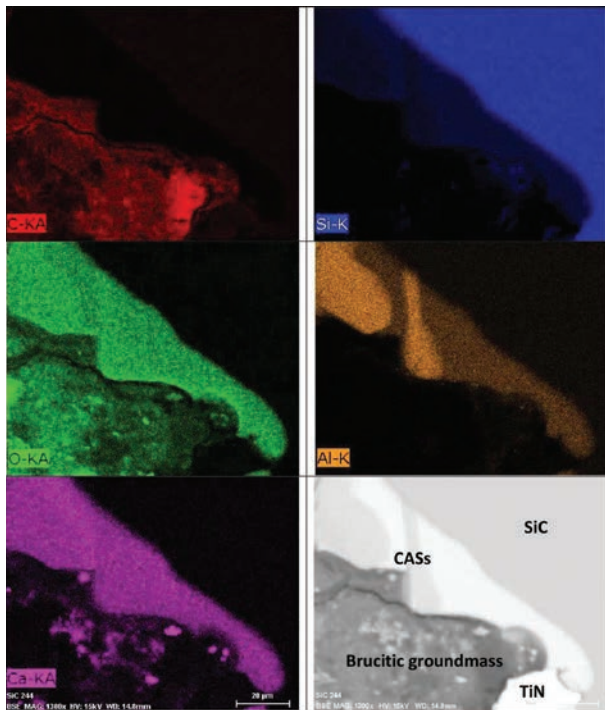


FIGURE 3. X-ray mapping of CAS inclusion in SiC no. 244. Dark lamellae in BSE image are dmisteinbergite (Table 1, analyses 10 and 11), while bright areas have a $\text{Ca}_{1-x}(\text{Al},\text{Si})_{2+x}\text{O}_5$ composition (Table 1, analyses 2 to 4). (Color online.)

occupy each about 50 vol% of the Ca-Al inclusions.

Microprobe analyses of CAS crystals have been carried out in fourteen moissanite grains and representative analyses are compiled in Table 1. Compositions are somewhat variable but at least eight different compounds can be distinguished.

The most common type of CAS inclusion consist of an association of dark lamellae of stoichiometric $\text{CaAl}_2\text{Si}_2\text{O}_8$ (Table 1) and bright lamellae of an unreported, apparently stoichiometric, $\text{Ca}_x(\text{Al},\text{Si})_{1-x}\text{O}_3$ phase (Table 1; Fig. 2). About 1–2 mol% of “celsiane”-component is found in the $\text{CaAl}_2\text{Si}_2\text{O}_8$ structure, which is also SrO-, SO_3 -, and LREE-bearing (up to 0.30 wt%; Table 1). $\text{CaAl}_2\text{Si}_2\text{O}_8$ shows main Raman modes at **120**, **225**, **330**, **442**, **508**, **807**, **897**, **917**, and **1126** cm^{-1} (in bold the strongest ones, see Fig. 4a), which corresponds to the pseudo-hexagonal polymorph (Daniel et al. 1995) named dmisteinbergite (Jambar and Vanko 1992; Sokol et al. 1998). Dmisteinbergite was also observed as the only mineral present in some inclusions. $\text{Ca}_x(\text{Al},\text{Si})_{1-x}\text{O}_3$ can contain up to 40.18 wt% of Al_2O_3 , while it is also BaO-, SrO-, SO_3 -, and LREE-bearing (up to 0.33 wt%; Table 1). This phase shows main Raman modes at 175, **416**, **1009**, and **1136** cm^{-1} (Fig. 4b).

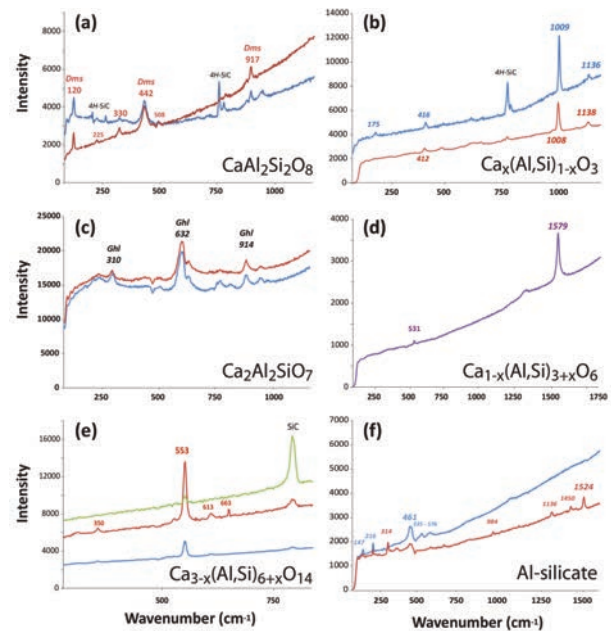


FIGURE 4. Raman spectra of Ca-Al-rich phases. (a) Spectra of dmisteinbergite inclusions (Dms), along with that of hosting 4H-SiC. Blue: pure dmisteinbergite in grain 244; red: dmisteinbergite in association with SiC-4H in grain 85. (b) Mixed spectra of $\text{Ca}_x(\text{Al},\text{Si})_{1-x}\text{O}_3$, along with that of hosting phase 4H-SiC. Blue: spectrum obtained in grain 85; red: spectrum obtained in grain 78. (c) Two pure spectra of gehlenite (Ghl) in grain 78 (both blue and red). (d) Spectrum of $\text{Ca}_{1-x}(\text{Al},\text{Si})_{3+x}\text{O}_6$. (e) Spectra of $\text{Ca}_{3-x}(\text{Al},\text{Si})_{6+x}\text{O}_{14}$ phase, along with that of hosting SiC (grain 27). Green: spectrum displaying a strong moissanite peak and a weaker $\text{Ca}_{3-x}(\text{Al},\text{Si})_{6+x}\text{O}_{14}$ peak; red: spectrum showing strong peak of $\text{Ca}_{3-x}(\text{Al},\text{Si})_{6+x}\text{O}_{14}$ and weak moissanite peak; blue: spectrum showing only weak $\text{Ca}_{3-x}(\text{Al},\text{Si})_{6+x}\text{O}_{14}$ peak. (f) Spectra of Al-silicate in grain 220. Blue: spectrum displaying mainly the strongest peaks at 461 cm^{-1} ; red: more detailed spectrum showing additional peaks and one pronounced at 1524 cm^{-1} . (Color online.)

TABLE 1. Microprobe analyses of CAS phases

No. of hosting SiC No. of μ -probe	Ca _{1-x} (Al,Si) _{3+x} O ₆			CaAl _{4-x} Si _x O ₇			Ca _x (Al,Si) _{1-x} O ₃							
	13 1	78 18	273 46	29 59	29 60	78 10	78 11	78 12	250 33	250 35	250 36	250 38	49 62	49 63
SiO ₂	18.01	20.87	28.16	5.66	4.72	37.77	34.37	32.59	37.08	37.99	37.21	37.56	36.92	36.25
TiO ₂	bd	bd	bd	bd	bd	bd	bd	bd	bd	bd	bd	bd	bd	bd
ZrO ₂	bd	bd	bd	bd	bd	bd	bd	bd	bd	bd	bd	bd	bd	bd
Al ₂ O ₃	58.73	64.01	56.86	75.06	76.15	39.02	39.62	40.18	35.22	35.52	35.29	35.01	26.11	28.29
Y ₂ O ₃	0.14	bd	bd	bd	bd	bd	bd	bd	bd	bd	0.07	0.07	bd	bd
La ₂ O ₃	bd	bd	bd	bd	bd	bd	0.08	bd	bd	bd	bd	0.13	bd	bd
Ce ₂ O ₃	bd	bd	bd	0.09	bd	bd	bd	bd	bd	bd	bd	0.13	bd	bd
FeO	bd	bd	0.09	bd	bd	0.15	bd	bd	bd	bd	bd	bd	bd	bd
MnO	bd	bd	bd	bd	bd	bd	bd	0.08	bd	bd	bd	bd	bd	bd
MgO	0.11	0.22	bd	bd	bd	0.13	0.08	0.07	0.14	0.05	0.04	0.09	0.16	0.23
CaO	25.02	15.10	13.49	21.24	21.51	22.52	25.61	27.09	27.16	26.74	24.22	25.91	36.27	35.31
SrO	0.07	bd	0.08	0.16	0.22	0.12	0.08	bd	bd	0.11	bd	0.09	0.40	0.45
BaO	0.21	0.14	0.33	0.22	0.06	0.62	1.07	0.93	1.04	0.59	1.25	1.05	0.82	0.23
Na ₂ O	bd	bd	0.09	bd	bd	0.08	0.11	0.14	0.04	0.05	0.04	0.07	0.33	0.34
K ₂ O	bd	0.03	0.06	bd	bd	0.06	0.12	0.14	0.03	bd	bd	0.06	0.03	bd
SO ₃	0.46	0.21	0.59	0.17	bd	0.42	0.71	0.77	0.42	0.99	1.22	0.46	0.20	bd
Total	102.75	100.58	99.77	102.60	102.66	100.89	101.85	101.99	101.13	102.08	99.34	100.63	101.24	101.10
Si	0.65	0.73	0.99	0.24	0.20	0.67	0.62	0.59	0.67	0.68	0.69	0.68	0.69	0.68
Ti	0.00	0.00	0.00	0.00	0.00	0.00	0.00	0.00	0.00	0.00	0.00	0.00	0.00	0.00
Zr	0.00	0.00	0.00	0.00	0.00	0.00	0.00	0.00	0.00	0.00	0.00	0.00	0.00	0.00
Al	2.49	2.64	2.34	3.71	3.76	0.82	0.84	0.86	0.75	0.75	0.77	0.75	0.58	0.62
Y	0.00	0.00	0.00	0.00	0.00	0.00	0.00	0.00	0.00	0.00	0.00	0.00	0.00	0.00
La	0.00	0.00	0.00	0.00	0.00	0.00	0.00	0.00	0.00	0.00	0.00	0.00	0.00	0.00
Ce	0.00	0.00	0.00	0.00	0.00	0.00	0.00	0.00	0.00	0.00	0.00	0.00	0.00	0.00
Fe	0.00	0.00	0.00	0.00	0.00	0.00	0.00	0.00	0.00	0.00	0.00	0.00	0.00	0.00
Mn	0.00	0.00	0.00	0.00	0.00	0.00	0.00	0.00	0.00	0.00	0.00	0.00	0.00	0.00
Mg	0.01	0.01	0.00	0.00	0.00	0.00	0.00	0.00	0.00	0.00	0.00	0.00	0.00	0.01
Ca	0.96	0.57	0.51	0.96	0.97	0.43	0.49	0.53	0.53	0.51	0.48	0.50	0.73	0.70
Sr	0.00	0.00	0.00	0.00	0.01	0.00	0.00	0.00	0.00	0.00	0.00	0.00	0.00	0.00
Ba	0.00	0.00	0.00	0.00	0.00	0.00	0.01	0.01	0.01	0.00	0.01	0.01	0.01	0.00
Na	0.00	0.00	0.01	0.00	0.00	0.00	0.00	0.00	0.00	0.00	0.00	0.00	0.01	0.01
K	0.00	0.00	0.00	0.00	0.00	0.00	0.00	0.00	0.00	0.00	0.00	0.00	0.00	0.00
S	0.01	0.01	0.02	0.01	0.00	0.01	0.01	0.01	0.01	0.01	bd	0.01	0.00	0.00
Σ cations	4.13	3.96	3.87	4.92	4.93	1.94	1.98	2.00	1.97	1.96	1.96	1.96	2.04	2.03
No. Oxygen	6	6	6	7	7	3	3	3	3	3	3	3	3	3

No. of hosting SiC No. of μ -probe	Ca ₂ Al ₂ SiO ₇ Ghelenite						CaAl ₂ Si ₂ O ₈ Dmisteinbergite											
	78 5	78 8	78 21	78 22	78 23	78 24	78 17	250 37	272 39	273 44	273 45	175 51	175 52	175 54	175 55	175 56	244 10	244 11
SiO ₂	23.48	22.62	25.43	21.98	24.73	25.06	40.41	40.37	40.52	44.53	43.87	40.69	42.48	44.06	41.61	43.83	44.06	40.59
TiO ₂	bd	bd	bd	bd	bd	bd	bd	bd	bd	0.06	0.08	bd						
ZrO ₂	bd	bd	bd	bd	bd	bd	bd	bd	bd	bd	bd	bd	bd	bd	bd	bd	bd	bd
Al ₂ O ₃	37.01	38.44	36.84	45.17	38.61	39.10	38.37	36.92	36.01	35.54	34.16	36.16	36.17	34.93	37.49	36.53	36.12	38.57
Y ₂ O ₃	bd	bd	bd	bd	bd	bd	bd	bd	bd	bd	bd	bd	bd	bd	bd	bd	bd	bd
La ₂ O ₃	bd	0.09	bd	bd	bd	bd	bd	bd	bd	bd	bd	bd	bd	bd	bd	bd	0.10	0.09
Ce ₂ O ₃	bd	bd	bd	bd	bd	bd	bd	bd	bd	bd	bd	bd	bd	0.14	bd	bd	0.19	bd
FeO	bd	bd	bd	bd	bd	bd	bd	bd	bd	0.39	0.29	bd	bd	0.27	0.13	0.11	bd	0.08
MnO	bd	bd	bd	bd	bd	bd	bd	bd	bd	bd	bd	bd	0.03	0.02	bd	bd	bd	
MgO	bd	bd	bd	bd	bd	bd	0.11	bd	0.06	bd	0.75	0.09	bd	0.08	0.05	bd	0.05	
CaO	40.09	38.21	38.10	32.91	36.38	36.49	20.20	20.43	21.94	18.07	18.16	20.89	19.47	19.85	20.63	19.62	19.67	19.52
SrO	bd	0.17	0.09	0.10	bd	0.08	0.08	0.09	0.15	0.08	0.06	0.12	bd	0.08	bd	bd	bd	
BaO	bd	0.32	0.18	0.33	0.33	0.16	0.79	1.33	1.33	0.54	0.58	0.99	0.79	1.75	1.07	0.82	0.44	0.49
Na ₂ O	bd	bd	0.06	0.04	bd	bd	bd	bd	0.05	0.19	0.16	0.04	bd	0.04	bd	0.08	0.09	
K ₂ O	bd	bd	bd	bd	bd	bd	0.07	bd	0.05	0.12	0.11	0.03	bd	0.03	bd	0.05	0.07	
SO ₃	0.09	0.24	0.26	0.64	0.22	0.14	0.16	0.24	0.12	2.20	1.50	0.86	bd	0.26	0.31	bd	0.04	bd
Total	100.67	100.09	100.96	101.17	100.27	101.03	100.19	99.38	100.17	101.79	99.74	99.81	99.03	101.40	101.46	100.91	100.75	99.55
Si	1.06	1.03	1.13	0.97	1.10	1.11	1.90	1.92	1.92	2.07	2.07	1.94	2.00	2.05	1.94	2.02	2.03	1.90
Ti	0.00	0.00	0.00	0.00	0.00	0.00	0.00	0.00	0.00	0.00	0.00	0.00	0.00	0.00	0.00	0.00	0.00	0.00
Zr	0.00	0.00	0.00	0.00	0.00	0.00	0.00	0.00	0.00	0.00	0.00	0.00	0.00	0.00	0.00	0.00	0.00	0.00
Al	1.96	2.06	1.94	2.34	2.03	2.04	2.12	2.07	2.02	1.95	1.90	2.03	2.01	1.92	2.06	1.99	1.97	2.13
Y	0.00	0.00	0.00	0.00	0.00	0.00	0.00	0.00	0.00	0.00	0.00	0.00	0.00	0.00	0.00	0.00	0.00	0.00
La	0.00	0.00	0.00	0.00	0.00	0.00	0.00	0.00	0.00	0.00	0.00	0.00	0.00	0.00	0.00	0.00	0.00	0.00
Ce	0.00	0.00	0.00	0.00	0.00	0.00	0.00	0.00	0.00	0.00	0.00	0.00	0.00	0.00	0.00	0.00	0.00	0.00
Fe	0.00	0.00	0.00	0.00	0.00	0.00	0.00	0.00	0.02	0.01	0.00	0.00	0.01	0.00	0.00	0.00	0.00	0.00
Mn	0.00	0.00	0.00	0.00	0.00	0.00	0.00	0.00	0.00	0.00	0.00	0.00	0.00	0.00	0.00	0.00	0.00	0.00
Mg	0.00	0.00	0.00	0.00	0.00	0.00	0.01	0.00	0.00	0.05	0.01	0.00	0.01	0.00	0.00	0.00	0.00	0.00
Ca	1.93	1.86	1.82	1.55	1.74	1.73	1.02	1.04	1.12	0.90	0.92	1.07	0.98	0.99	1.03	0.97	0.97	0.98
Sr	0.00	0.00	0.00	0.00	0.00	0.00	0.00	0.00	0.00	0.00	0.00	0.00	0.00	0.00	0.00	0.00	0.00	0.00
Ba	0.00	0.01	0.00	0.01	0.01	0.00	0.01	0.02	0.02	0.01	0.01	0.02	0.01	0.03	0.02	0.01	0.01	0.01
Na	0.00	0.00	0.00	0.00	0.00	0.00	0.00	0.00	0.02	0.01	0.00	0.00	0.00	0.00	0.00	0.00	0.01	0.01
K	0.00	0.00	0.00	0.00	0.00	0.00	0.00	0.00	0.01	0.01	0.00	0.00	0.00	0.00	0.00	0.00	0.00	0.00
S	0.00	0.01	0.00	0.01	0.01	0.00	0.01	0.01	0.00	0.08	0.05	0.03	0.00	0.01	0.01	0.00	0.00	0.00
Σ cations	4.97	4.96	4.90	4.87	4.89	4.88	5.07	5.08	5.10	5.06	5.05	5.10	5.01	5.03	5.07	5.00	5.00	5.05
No. Oxygen	7	7	7	7	7	7	8	8	8	8	8	8	8	8	8	8	8	8

(Continued on next page)

TABLE 1.—CONTINUED

No. of hosting SiC No. of μ -probe	Ca _{1-x} (Al,Si) _{2+x} O ₅						Al-bearing SiO ₂		Ca _{3-x} (Al,Si) _{6+x} SiO ₁₄
	244	244	244	272	272	272	220	220	49
SiO ₂	56.75	49.40	51.59	61.88	59.03	62.31	65.39	66.39	43.04
TiO ₂	bd	bd	bd	bd	bd	bd	bd	bd	bd
ZrO ₂	0.21	0.34	0.34	bd	bd	bd	0.90	0.86	bd
Al ₂ O ₃	15.45	14.97	14.85	20.10	21.84	20.01	17.65	17.22	25.38
Y ₂ O ₃	0.52	1.05	0.98	bd	0.11	bd	bd	bd	bd
La ₂ O ₃	0.14	0.18	0.36	bd	bd	bd	bd	bd	bd
Ce ₂ O ₃	0.36	0.76	0.72	0.08	0.09	bd	0.37	0.44	0.11
FeO	bd	bd	bd	bd	bd	bd	bd	bd	bd
MnO	bd	0.11	0.10	bd	bd	bd	bd	bd	bd
MgO	0.33	0.45	0.48	0.06	0.10	0.07	0.14	0.17	0.43
CaO	19.49	23.08	23.07	14.43	16.12	14.08	1.67	1.70	27.37
SrO	bd	bd	bd	0.07	bd	bd	bd	bd	0.81
BaO	2.94	2.77	2.94	1.24	1.19	1.19	5.97	6.04	1.00
Na ₂ O	bd	0.09	0.12	0.20	0.19	0.20	0.81	0.71	0.28
K ₂ O	0.46	0.28	0.24	0.20	0.17	0.20	2.01	2.21	0.06
SO ₃	1.10	1.99	1.94	2.15	2.01	2.00	3.02	2.91	0.21
F	1.60	3.91	3.80	na	na	na	na	na	na
Cl	0.04	0.05	bd	na	na	na	na	na	na
Total	99.39	99.43	101.53	100.41	100.85	100.06	97.93	98.65	98.69
Si	1.75	1.64	1.66	1.77	1.69	1.77	3.15	3.17	3.74
Ti	0.00	0.00	0.00	0.00	0.00	0.00	0.00	0.00	0.00
Zr	0.00	0.01	0.01	0.00	0.00	0.00	0.02	0.02	0.00
Al	0.56	0.58	0.56	0.68	0.74	0.67	1.00	0.97	2.60
Y	0.01	0.02	0.02	0.00	0.00	0.00	0.00	0.00	0.00
La	0.00	0.00	0.00	0.00	0.00	0.00	0.00	0.00	0.00
Ce	0.00	0.01	0.01	0.00	0.00	0.00	0.01	0.01	0.00
Fe	0.00	0.00	0.00	0.00	0.00	0.00	0.00	0.00	0.00
Mn	0.00	0.00	0.00	0.00	0.00	0.00	0.00	0.00	0.00
Mg	0.02	0.02	0.02	0.00	0.00	0.00	0.01	0.01	0.06
Ca	0.64	0.82	0.80	0.44	0.50	0.43	0.09	0.09	2.55
Sr	0.00	0.00	0.00	0.00	0.00	0.00	0.00	0.00	0.04
Ba	0.04	0.04	0.04	0.01	0.01	0.01	0.11	0.11	0.03
Na	0.00	0.01	0.01	0.01	0.01	0.01	0.08	0.07	0.05
K	0.02	0.01	0.01	0.01	0.01	0.01	0.12	0.13	0.01
S	0.03	0.05	0.05	0.05	0.04	0.04	0.11	0.10	0.01
Σ cations	3.06	3.20	3.18	2.97	2.95	2.95	4.70	4.69	9.09
No. Oxygen	5	5	5	5	5	5	8	8	14

Note: bd = below detection; na = not analyzed.

In a second association, dmisteinbergite occurs associated in a bright and dark lamellae structure with stoichiometric Ca_{1-x}(Al,Si)_{2+x}O₅ (Table 1; Fig. 3). This phase can accommodate up to 21.84 wt% of Al₂O₃, while it is also BaO-, SO₃-, LREE- (up to 2.05 wt%), F- (up to 3.91 wt%), and Cl-bearing (Table 1). No detectable Raman modes are active for Ca_{1-x}(Al,Si)_{2+x}O₅ phase. It has also been found in contact to TiN (osbornite; Fig. 3).

Stoichiometric, Mg- and Fe-free, but BaO-, SrO-, and SO₃-bearing gehlenite, Ca₂Al₂SiO₇ (Table 1) has been found bordering three moissanite crystals. The studied gehlenite shows Raman modes at 182, 221, 248, **310**, **632**, 658, 798, **914**, 982, and 1009 cm⁻¹ (Fig. 4c), which fits literature data (Sharma et al. 1983; Bouhifd et al. 2002). Gehlenite-like composition has been also reported from a grain included in moissanite from Luobusa (Robinson et al. 2004).

Four other CAS and AS compositions have been measured with the microprobe, either occurring as single inclusions or associated to dmisteinbergite.

The first mineral is a silica-bearing Ca-aluminate, with the stoichiometry of CaAl_{4-x}Si_xO₇. The mineral is also BaO-, SrO-, and SO₃-bearing (Table 1) and shows weak Raman modes at 118, 138, 252, 303, 326, 412, 458, and 1125 cm⁻¹. The mineral is compositionally comparable to grossite, CaAl₄O₇ (e.g., Boyko

and Wisnyi 1958; Weber and Bischoff 1994), but the Raman spectrum obtained is not in agreement with data reported by Hofmeister et al. (2004).

A second CAS phase has a composition of Ca_{1-x}(Al,Si)_{3+x}O₆, close to that of the pyroxene kushiroite, CaAl₂SiO₆. This phase also contains BaO, SrO, SO₃, and traces of LREE (Table 1). It shows weak Raman modes at 239, 291–301, 326–347, 546–548, 604, 622–626, and 966 cm⁻¹ on one grain, and strong Raman modes at **531** and **1579** cm⁻¹ on a second grain (Fig. 4d).

The third unreported CAS phase has a Ca_{3-x}(Al,Si)_{6+x}O₁₄ composition. This phase also bears BaO, SrO, SO₃, and Ce₂O₃ (Table 1), and shows main Raman modes at 351, **553**, and 613 cm⁻¹ (Fig. 4e).

The fourth phase, included as single grain within a moissanite crystal, is an Al-silicate; SiO₂ averages 65.9 wt%, while Al₂O₃ averages 17.4 wt%; the phase also contains 3 wt% alkalis, 6 wt% BaO, 2 wt% SO₃, <2 wt% CaO+MgO, almost 0.9 wt% ZrO₂ and up to 0.53 wt% LREE (Table 1). This phase shows main Raman modes at 147, 216, 283, 314, **461**, 535, 576, 671, 984, 1136, 1450, and 1524 cm⁻¹ (Fig. 4f), with the strongest peak at **461** cm⁻¹, close to that of quartz. Oleynikov et al. (1987, Table 2, p. 158) reported Mg-free alumina-silicate phase with a very similar composition, namely (microprobe data) SiO₂ 78.80–93.17 wt%, Al₂O₃ 3.05–11.26 wt%, K₂O 0.77–5.15 wt%, Na₂O 0.48–1.98 wt%, CaO 0.19–0.41 wt%, FeO 0.21–0.74 wt%, and TiO₂ 0.09–0.35 wt%. This hundred-micrometer-sized, tabular phase, along with silicides, was found included in moissanite from heavy-mineral separates from mafic rocks from Russia.

In summary, the tabular, xenomorphic, or drop-shaped hundred-micrometer-sized CAS and AS inclusions in moissanite show exsolution lamellae of the following types: (1) dmisteinbergite (hexagonal modification of CaAl₂Si₂O₈; n = 15), in association with either Ca_x(Al,Si)_{1-x}O₃ (n = 8) or Ca_{1-x}(Al,Si)_{2+x}O₅ (n = 4), or even dmisteinbergite alone and (2) gehlenite (n = 3); (simplified) CaAl_{4-x}Si_xO₇ (n = 1); Ca_{1-x}(Al,Si)_{3+x}O₆ (n = 5); Ca_{3-x}(Al,Si)_{6+x}O₁₄ (n = 3); and Al-bearing SiO₂ (n = 1), mainly as single minerals, either included in, or rimming moissanite crystals. All CAS phases are variably enriched in Ba, Sr, S, LREE, and Zr (Table 1), and most of them show distinctive Raman modes and spectra.

MgO and FeO contents are in all analyzed CAS phases at or below the detection limit, with maximum MgO contents of 0.75 wt% in one analysis of dmisteinbergite, and maximum FeO content of 0.39 wt% in another dmisteinbergite analysis. This is coherent with literature data predicting iron-free silicates in equilibrium with SiC (Mathez et al. 1995; Ulmer et al. 1998).

DISCUSSION

The data demonstrate that the CaAl-silicates inclusions hosted in moissanite crystals cannot be synthetic because of the thermodynamic incompatibility between the α -modification of SiC, above 1900 °C, and condensation temperatures of potentially

present CAS phase, below 1500 °C (Zhou and Telle 2010). Moreover, most of the analyzed CAS phases included in moissanite are LREE-bearing, in some cases also fluorine-bearing. This is definitely not compatible with the Acheson synthesis conditions. One particular phase, containing >66 wt% SiO₂ and showing a close-to-quartz Raman spectrum (Fig. 4f), might have existed in the Acheson mixture at room conditions, but could not have survived as inclusion within SiC without having been reduced to carbide or silicide. As already stated, neither CAS nor any kind of oxide is reported from the synthetic SiC literature. The only phases reported in synthetic material are silicides, boron-carbides, and amorphous carbon precipitates (e.g., More et al. 1986; Backhaus-Ricoult et al. 1993; Munro 1997).

The association of CAS phases as inclusions in moissanite opens new questions about the *P-T* conditions of formation. Given that our moissanite occurrence is comparable to occurrences in kimberlites and other diamond-bearing assemblages (see introduction), it is obvious to claim pressure as the stabilizer “ingredient” of the observed CAS association. We will therefore review whether the here-reported CAS phases are ultrahigh-pressure phases.

The CaO-Al₂O₃-SiO₂ system

The liquidus surface of the well-studied ternary CaO-Al₂O₃-SiO₂ system (e.g., Osborn and Muan 1960; Mao et al. 2006) at ambient pressure is shown in Figure 5. The plotted points are analyses of CAS phases found in this study, in weight percent. Coexisting phases are connected with tie lines.

Gehlenite analyses plot in the stability field of gehlenite and dmisteinbergite in the stability field of anorthite, while all the other compositions do not fit any of the ambient-pressure stability fields. These latter are therefore either quenched melt inclusion, or they represent high-pressure (HP) phases that may have crystallized from melt inclusions. The former option can be discarded because Ca_x(Al,Si)_{1-x}O₃, Ca_{1-x}(Al,Si)_{3+x}O₆, Ca_{3-x}(Al,Si)_{6+x}O₁₄, and the Al-bearing SiO₂ phases show active Raman modes with sharp peaks (Fig. 4), indicative of crystallinity. However, not all Raman spectra (Fig. 4) do fit known phases in the CAS system.

Dmisteinbergite was found in pyrometamorphic rocks from the Chelyabinsk coal basin, Southern Urals (Sokol et al. 1998), in pseudotachylyte from the Gole Larghe Fault, Italian Alps (Nestola et al. 2010), and very recently also from the Allende meteorite (Ma et al. 2013). Dmisteinbergite crystallizes from a rapidly quenched silicate melt at ambient pressure at 1200–1400 °C instead of anorthite (Abe et al. 1991; Daniel et al. 1995). It is not clear whether very low oxygen-fugacity conditions help stabilize the metastable hexagonal and orthorhombic CaAl₂Si₂O₈ polymorphs (Sokol et al. 1998, and reference therein). The upper *P* stability limit of dmisteinbergite is not reported in the literature.

Anorthite has been used as starting material in numerous HT-HP experiments aimed at characterizing Ca-Al-silicate stability in the upper mantle (see below). Anorthite remains stable up to 17.5 GPa and 1500 °C (Gautron and Madon 1994), above which it decomposes to an assemblage of “distorted” anorthite with an hollandite-type HP structure, Al-rich CaSiO₃ with a perovskite-structure, and kyanite, according to the following reaction:

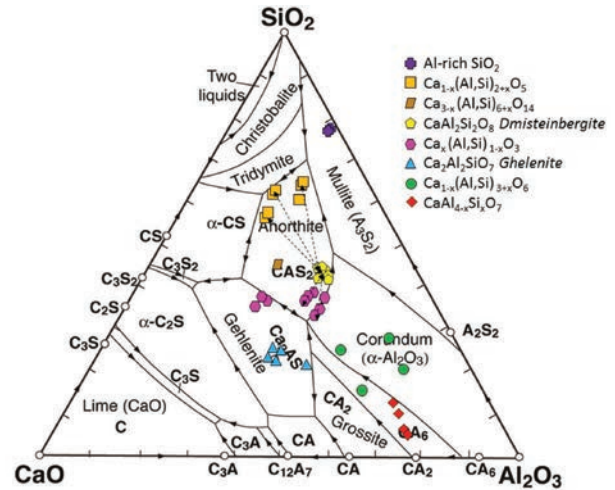
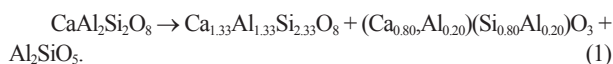


FIGURE 5. Ternary plot of the CAS analyses, in wt%, highlighting the presence of eight different compositions. In the background, the liquidus surface of SiO₂-CaO-Al₂O₃ system at ambient pressure (Osborn and Muan 1960) is shown. The arrows indicate the direction of downward temperature gradient. In the cement chemistry jargon, “C” stands for CaO, “A” for Al₂O₃, and “S” for SiO₂ (example: CAS₂ = CaO + Al₂O₃ + 2SiO₂ = CaAl₂Si₂O₈ = anorthite). (Color online.)

Gehlenite is a highly refractory mineral occurring in HT metamorphic peraluminous rocks that underwent calcium metasomatism and HT contact aureoles in impure limestone. The nearly pure, Fe- and Mg-free end-member has been mainly reported from carbonaceous chondrites (e.g., Zhang and Hsu 2009; Simon and Grossman 2011). Experimental work has shown that the assemblage gehlenite, anorthite, and liquid is stable up to 2.5 GPa and 1400 °C, above which it breaks down to grossular, Ca₃Al₂Si₃O₁₂ (Surkov and Doroshev 1998).

Grossular has been also extensively used as a starting material in HP-HT experiments, recently reviewed by Kawai and Tsuchiya (2012), to constrain stability fields of Ca- and Al-hosting silicates in subducted sediments and continental rocks down to upper mantle and greater depths. Ahmed-Zaid and Madon (1995) used a diamond-anvil cell (DAC) and transmission electron microscopy (TEM) to study the breakdown of pure, natural grossular at 40 and 50 GPa according to the reaction:



Experiments were conducted at temperatures above 1100 ± 400 K. The 8 mol% Al₂O₃-bearing CaSiO₃ phase was found to be amorphous, while CaAl₂SiO₆ was crystalline, but did not show the Ca-tschermakite pyroxene structure. At estimated temperatures of 2200 ± 800 K, they reported the following reaction:



In these experiments, the 9 mol% Al₂O₃-bearing CaSiO₃ phase was amorphous, while Al₂SiO₅ was a new polymorph with titanite structure, along with crystalline CaO.

Yusa et al. (1995) conducted DAC experiments at 30.2 GPa

and 1000–1500 °C and reported the appearance of a new, unquenchable garnet polymorph of grossular composition, but in situ X-ray diffraction showed that the phase has a *Pbnm* orthorhombic symmetry comparable to MgSiO₃ perovskite.

Takafuji et al. (2002) used a multi-anvil press (MAP) coupled to synchrotron μ -XRD and analytical TEM to study in situ and quenched reaction products of synthetic grossular at 23–25 GPa and 1000–1600 K. In the quenched experiments, they found different associations of 8–25 mol% of an Al₂O₃-bearing CaSiO₃ phase alternating with lamellae of amorphous material and a “LiNbO₃-type” perovskite-structured phase. The authors noted that the Al solubility in CaSiO₃-perovskite decreased with increasing temperature (see also Kurashina et al. 2004; Komabayashi et al. 2007), and suggested that under unquenched conditions the amorphous phase had cubic symmetry, while the “LiNbO₃-type” was orthorhombic.

By studying the potential incorporation of uranium and thorium in silicates at mantle *P-T* conditions and using glass of grossular composition as starting material, Gréaux et al. (2009, 2011a, 2012) carried out DAC and MAP experiments at 19–26 GPa and 700–2000 K. Run products were characterized either in situ by μ -XRD or in quenched experiments by TEM. Gréaux and coworkers produced Al-rich CaSiO₃ perovskite containing 10.6–24.2 wt% Al₂O₃. In their runs, excess alumina was accommodated in the CAS-phase CaAl₄Si₂O₁₁.

CaAl₄Si₂O₁₁ was first reported by Irifune et al. (1994) while studying the decomposition of continental sediments at *P-T* conditions of the Transition Zone. Hirose et al. (1999) found as a liquidus phase of mid-ocean ridge basalt (MORB) exposed to 26–27 GPa and approximately 2500 K, respectively. A related Na-bearing CAS-phase, (Ca_xNa_{1-x})Al_{3+x}Si_{3-x}O₁₁, was also reported as natural mineral occurring in melt pockets of the heavily shocked martian meteorite NWA 856 (Beck et al. 2004). Zhai and Ito (2008) studied the *P-T* stability of this CAS-phase at 10–23 GPa and 1000–1600 °C. CaAl₄Si₂O₁₁ was found stable above 10 GPa and 1500 °C, with the boundary of its breakdown products grossular + corundum + stishovite showing a negative *dP/dT* slope. The upper stability of CaAl₄Si₂O₁₁ lies at approximately 30 GPa and 2000 K, where it dissociates to an assemblage of Al-rich CaSiO₃ with perovskite structure, corundum, and stishovite (Ishibashi et al. 2008; Gréaux et al. 2011b). Gautron et al. (1999) refined the structure of their CAS-phase as CaAl₄Si₂O₁₁ and found it isostructural with BaFe₄Ti₂O₁₁.

Another important HP-HT CAS-phase is CaAl₁₂Si₄O₂₇, experimentally synthesized at 14 GPa and 1550 °C by Gray et al. (2000). Gray et al. (2000) considered their CAS-phase CaAl₁₂Si₄O₂₇ to be isostructural with BaFe₁₁Ti₅O₂₃. These latter authors suggested that the BaO-Fe₂O₃-TiO₂ ambient-pressure system might be an analog to the CaO-Al₂O₃-SiO₂ high-pressure one, where the silicon is sixfold coordinated in a rutile-type structure. Given the complexity of the BaO-Fe₂O₃-TiO₂ system with at least 17 known phases (Vanderah et al. 1996, and reference therein), there is still a high probability to find additional new phases in the HP CaO-Al₂O₃-SiO₂ system (Gautron et al. 1999; Gray et al. 2000).

The Al-poor HP-HT CaSiO₃ system is well constrained, too (Kanzaki et al. 1998; Wang and Weidner 1994; Gasparik et al. 1994; Swamy and Dubrovinsky 1997; Shim et al. 2000; Akaogi

et al. 2004; Komabayashi et al. 2007). LP-HT wollastonite, CaSiO₃, and its HT polymorph pseudo-wollastonite, Ca₃Si₃O₉ (Seryotkin et al. 2012), undergo displacive phase transition to Ca₃Si₃O₉ with walstromite-structure at around 3–4 GPa (Joswig et al. 2003; Barkley et al. 2011; Liu et al. 2012). With increasing pressure, walstromite-structured Ca₃Si₃O₉ dissociates at 9–11 GPa to larnite, β -Ca₂SiO₄, and titanite-structured CaSi₂O₅ (Angel et al. 1996, 1997, 1999; Kudoh and Kanzaki 1998; Stebbins and Poe 1999; Schoenitz et al. 2001; Sueda et al. 2006). Larnite and CaSi₂O₅ are thought to be important REE-carriers at mantle depths (Wang et al. 2000; Dörsam et al. 2009). Experimental work also confirmed the assemblage walstromite-structured Ca₃Si₃O₉, β -larnite + titanite-structured CaSi₂O₅ in natural diamonds from Guinea (Joswig et al. 1999; Stachel 2001; Nasdala et al. 2003; Brenker et al. 2005). Above 14–15 GPa and 1600 °C, this assemblage further recomposes to more compact CaSiO₃ with perovskite-structure.

At even higher *P* and by adding alumina to the system, the CaSiO₃ perovskite-structured phase is replaced by a rhombohedral Ca₂AlSiO_{5.5} phase that possesses ordered oxygen defects. It is stable at 16 GPa and 1973 K (Bläss et al. 2007; Kojitani et al. 2009).

By increasing the Al₂O₃/CaO ratio, kushiroite, CaAl₂SiO₆, a Mg- and Fe-bearing pyroxene containing up to 88 mol% of Ca-tschemmakite becomes stable. The Ca-tschemmakite end-member *P-T* stability field has been constrained experimentally above 1.8 GPa and 1300 °C (Okamura et al. 1974; Ahmed-Zaid and Madon 1995; Surkov and Doroshev 1998). Kushiroite was found in the meteorites ALH 85085 (Kimura et al. 2009), Allende, Murray, and other carbonaceous chondrites (Ma et al. 2009) that did not undergo high-pressure metamorphism.

The Raman spectra of dmisteinbergite and gehlenite fit those of literature (Nestola et al. 2010; Bouhifd et al. 2002). However, a direct link between X-ray characterized HP-HT CAS phases and our Raman-constrained data is not yet made. The collected Raman spectra of Ca_{1-x}(Al,Si)_{3+x}O₆ (Fig. 4d) do not fit that of kushiroite (Kimura et al. 2009) nor Ca-tschemmakite (Sharma et al. 1983). Similarly, the CaAl_{4-x}Si_xO₇ Raman spectra do not fit grossite, CaAl₄O₇ (Hofmeister et al. 2004).

Based on their compositions, however, there are striking analogies between the here-reported CaAl-silicates and the above-reported HP-HT phases from the literature. For instance, the Ca_x(Al,Si)_{1-x}O₃ phase reported here contains up to 25 mol% of Al₂O₃ (Table 1), which corresponds to the maximum solubility of alumina within the perovskite-structured CaSiO₃ of Takafuji et al. (2002) or Gréaux et al. (2009, 2011a, 2011b). Ca_{1-x}(Al,Si)_{3+x}O₆ compositions reported in Table 1 are closely stoichiometric Ca-tschemmakite. The Ca_{1-x}(Al,Si)_{2+x}O₅ phase, which contain up to 2 wt% REE, ~3% BaO, ~4 wt% F, >1.7 wt% SO₃, and 0.34 wt% ZrO₂ is comparable to the data and predictions of Dörsam et al. (2009) suggesting that these phase can be the mantle repository for large ion lithophile elements (LILE) and LREE. Our Ca_{3-x}(Al,Si)_{6+x}O₁₄ phase, furthermore, written with its actual stoichiometry derived from its microprobe analysis (Table 1, no. 65), namely Ca_{2.55}Al_{2.60}Si_{3.74}O₁₄, might recall closely phase Ba₃Fe₂Ti₄O₁₄ reported by Vanderah et al. (1996) and refined in the *C2/m* space group, with which it might be isostructural. Likewise the HP phase CaAl₁₂Si₄O₂₇ of Gray et al. (2000) is isostructural with BaFe₁₁Ti₅O₂₃, and CaAl₄Si₂O₁₁ of Gautron et al. (1999) is

isostructural with $\text{BaFe}_4\text{Ti}_2\text{O}_{11}$ (see previous discussion).

The short review provided above considered single, stoichiometric, either quenched or in situ equilibrated minerals. We recall that the here-reported CAS inclusions in moissanite mainly consist of two phases, where one phase forms exsolution lamellae in a second. In the literature (i.e., Takafuji et al. 2002; Yamamoto et al. 2009; Gréaux et al. 2011a, 2011b; Nishi et al. 2011) such a textural relationship is interpreted as retrograde transformation in association with volumetric changes occurring during upwelling and decompression (e.g., Alifirova et al. 2012, and reference therein).

This, in turn, means that the parental minerals that transformed to the here observed associations (modal abundance in parentheses): (a) dmisteinbergite (~50 vol%) + $\text{Ca}_x(\text{Al},\text{Si})_{1-x}\text{O}_3$ (~50 vol%; Fig. 2), (b) or dmisteinbergite (~50 vol%) + $\text{Ca}_{1-x}(\text{Al},\text{Si})_{2+x}\text{O}_5$ (~50 vol%; Fig. 3) should have been even denser phases, whose stoichiometry might be found within the HP-HT CaO-Al₂O₃-SiO₂ system.

Further combined structural and Raman studies of the presented phases, as well as experimental work on hypothetical compositions are strongly needed to explore the CaO-Al₂O₃-SiO₂ system at high pressures.

Hypotheses on moissanite and CAS origins

Several findings of moissanite have been reported, either as genetically linked to sub-surface phenomena, such as impact craters (i.e., Moissan 1905; Hough et al. 1995) or forest fires (Sameshima and Rodgers 1990), or predicted as a thermodynamically stable phase growing during lightning strikes (Essene and Fisher 1986). Most moissanite occurrences, however, have been reported from rocks of deep-mantle provenance, such as kimberlites, lamproites, and peridotites (ophiolites), and their narrow association with diamonds has been unambiguously proved (Mathez et al. 1995; Trumbull et al. 2009; Shiryayev et al. 2011, and references therein).

Although authors often speculate about the enigmatic and unsolved origin of natural, terrestrial silicon-carbide, there is a general strong consensus on two points:

(1) Moissanite stability is restricted to extremely low oxygen fugacity (f_{O_2}) conditions, computed or experimentally determined at five to six log units below the iron-wüstite (IW) oxygen buffer (Essene and Fisher 1986; Mathez et al. 1995; Ulmer et al. 1998; Dobrzhinetskaya and Green 2007; Takahashi et al. 2013; Shiryayev and Gaillard 2014; Schmidt et al. 2014).

(2) Moissanite shows strongly depleted $\delta^{13}\text{C}$ values, ranging from -18 to -35‰ for ophiolite suites, from -21 to -31‰ for the Turkish pebble suite (Trumbull et al. 2009), and from -22 to -30‰ for the kimberlitic suites of Marshintsev (1990), Leung et al. (1990), and Mathez et al. (1995). These values are in strong contrast with $\delta^{13}\text{C}$ values of peridotitic and the large majority of eclogitic diamond suites (Shirey et al. 2013), plotting around -5‰ and considered as the “normal” mantle range. The moissanite values, instead, better fit the $\delta^{13}\text{C}$ values of diamonds from ophiolites, ranging -18 to -28‰ (Yang et al. 2014). These diamonds, very often associated to moissanite, are interpreted as originated from the Transition Zone (Yang et al. 2014).

Based on these facts, several hypotheses for a deep-mantle origin of moissanite and hence also the CAS and AS inclusions

in moissanite they contain is proposed. Mathez et al. (1995) proposed that moissanite might have an upper mantle origin, where it might be confined to microenvironments with f_{O_2} conditions lower than IW values. They also proposed that the origin of moissanite might be genetically linked to subduction of biogenic carbon. This scenario would be consistent with the C and N isotopes signature, while reducing conditions necessary for SiC formation would be provided by serpentinization processes (Mathez et al. 1995; Ulmer et al. 1998).

Moissanite with CAS inclusions could have a pristine origin from primordial Earth and would be located mostly in the Lower Mantle. This hypothesis was first raised by Mathez et al. (1995) based on the assumptions that Earth Core formation required lower-than-IW f_{O_2} conditions (see also Hin et al. 2014) that current f_{O_2} conditions of the lower mantle are not well-known, and that H- and L-ordinary chondrites and achondrites show $\delta^{13}\text{C}$ values of -20 to -32‰. The pristine moissanite origin hypothesis has been also suggested by Hugh Rollinson (pers. comm. 2009, in Trumbull et al. 2009), based on analogy of $\delta^{13}\text{C}$ values of 12 martian meteorites of $-20 \pm 4\%$ (Grady et al. 2004) and the average values of terrestrial moissanite. This scenario was recently supported by Horita and Polyakov (2015) using carbon budget modeling.

More recently, Hazen et al. (2013) proposed that moissanite might have formed during the giant impact formation of the Earth's Moon since mantle material was exposed to vacuum of space, simultaneously to very HT regimes.

Even though we still miss many experimental data to constrain with certainty the high-pressure origin of the moissanite-bearing phases studied here, Ca-Al-silicates found as inclusions in SiC described in this study are a unique proxy to tentatively explain a possible origin. We speculated about their HP-HT origin already, but there is another striking feature that characterizes the association of CAS-phases with SiC. All analyzed phases are unexpectedly Mg-free. Moissanite, silicon metal and iron-silicides previously characterized in the same sample (Di Pierro et al. 2003) are all also Mg-free. This strongly contrasts with the surrounding brucite-dominated groundmass of the sample, crowded with MgFe-silicates and chromian spinel. This would suggest that the reduced phases, moissanite, silicon, and silicides, and associated Mg-free CaAl-silicates form a separate paragenesis, possibly not in equilibrium with the surrounding ultramafic matrix.

Dmisteinbergite (Ma et al. 2013), kushiroite (Kimura et al. 2009), and ghelenite (Nomura and Miyamoto 1998; Krot et al. 2004; Zhang and Hsu 2009; Simon and Grossman 2011) have all been extensively reported from Ca-Al-inclusions (CAIs) in chondrites, and were interpreted as pristine minerals witnessing the early stages of formation of the Solar System. Moreover, traces of micrometer-sized, cubic silicon-carbide grains of presolar origin have been extensively reported from carbonaceous chondrites as well (see Daulton et al. 2002, for a review). One could therefore speculate that during the early accretion steps of our planet, significant traces of refractory moissanite and CaAl-silicates might have coexisted (Hazen et al. 2008; Marakushev et al. 2013) and become commonly scattered at different mantle depths. Kimberlite-like volcanism might have ultimately brought up to surface these double, composite parageneses. This scenario

would fit simultaneously the previously listed constraints such as the lower-than-IW f_{O_2} conditions, the strongly depleted $\delta^{13}C$ values not fitting the mantle values of peridotitic and most of eclogitic diamonds but those of pristine meteorites. However, moissanite grains are only known from unequilibrated primitive chondrites but not from higher-grade metamorphic, equilibrated chondrites (Brearley and Jones 1998). For this reason, it seems thermodynamically impossible that such tiny moissanite grains of meteoritic origin could have survived in the hot terrestrial mantle.

The Si isotope distribution between moissanite, silicon metal and silicides, and of course CAS phases, would be helpful to discern between a common origin or not for this association, and REE pattern of the CaAl-silicates could be helpful to support such a scenario (Shiryayev et al. 2011).

IMPLICATIONS

Hundred-micrometer-sized grains consisting of crystalline Ca-Al-silicates and Al-silicates have been found as inclusions in moissanite that has lower mantle $\delta^{13}C$ isotopic signature (Trumbull et al. 2009; Horita and Polyakov 2015), providing an additional criterion to distinguish natural moissanite from synthetic SiC.

A deep-mantle origin is supported by the fact that together with dmsteinbergite and gehlenite, the unreported phases $Ca_x(Al,Si)_{1-x}O_3$, $Ca_{1-x}(Al,Si)_{3+x}O_6$, $Ca_{1-x}(Al,Si)_{2+x}O_5$, $CaAl_{4-x}Si_xO_7$, $Ca_{3-x}(Al,Si)_{6+x}O_{14}$, and Al-bearing SiO_2 are found. The exsolution relationship, moreover, indicates that the parental minerals might have been even denser phases of the CAS system. Moreover, there are striking analogies between the CAS inclusions and HP-HT CAS phases reported in the literature. Whereas significant amounts of Ba, S, LREE, and in some of them also F, Cl, alkalis, and Zr, may have stabilized the CAS-phases to lower pressure conditions, they confirm predictions of Dörsam et al. (2009) that such minerals could be important sinks for LREE and LILE in the deep mantle.

Several high-pressure phases of the $CaO-Al_2O_3-SiO_2$ system are isostructural (e.g., Gray et al. 2000) with 1 of the 17 known members of the low-pressure $BaO-Fe_2O_3-TiO_2$ system (e.g., Vanderah et al. 1996). Considering that in the studied sample alone five unknown minerals of the $CaO-Al_2O_3-SiO_2$ system are present, it seems likely that exploration of the $CaO-Al_2O_3-SiO_2$ at high pressure will lead to the discovery of additional CAS phases.

ACKNOWLEDGMENTS

Salvatore Musacchia, the person who found the bluish pebble, is greatly acknowledged for providing the material for research. Electron-microprobe analyses at the University of Bern were supported by Schweizerischer Nationalfonds (credit 21-26579.89). Financial support from the Swiss National Science Foundation Commission of the University of Fribourg (fellowship n. PBF2-101389) to S.D.P. when he was a post-doc fellow at ENS/Lyon is greatly acknowledged. We thank Bruno Reynard, Isabelle Daniel, and Gilles Montagnac at ENS/Lyon for discussions and Raman lab assistance, and Philippe Grandjean at University Claude Bernard Lyon-1 for WDS-microprobe assistance. Jessy Gillot at Saint-Gobain Recherche is also thanked for the SEM-EDS X-ray mapping of CAS. We also thank Ed Mathez, an anonymous reviewer, and Associate Editor Daniel Hummer for their constructive reviews.

REFERENCES CITED

Abe, T., Tsukamoto, K., and Sunagawa, I. (1991) Nucleation, growth and stability of $CaAl_2Si_2O_8$ polymorphs. *Physics and Chemistry of Minerals*, 17, 473–484.
 Ahmed-Zaid, I., and Madon, M. (1995) Electron microscopy of high-pressure phases synthesized from natural garnets in a diamond-anvil cell: Implications for the min-

eralogy of the lower mantle. *Earth and Planetary Science Letters*, 129, 233–247.
 Akaogi, M., Yano, M., Tejima, Y., Iijima, M., and Kojitani, H. (2004) High-pressure transitions of diopside and wollastonite: Phase equilibria and thermochemistry of $CaMgSi_2O_6$, $CaSiO_3$ and $CaSi_2O_7$ - $CaTiSiO_5$ system. *Physics of the Earth and Planetary Interiors*, 143–144, 145–156.
 Aldanmaz, E., Köprübaşı, N., Güler, F., Kaymakçı, N., and Gourgaud, A. (2006) Geochemical constraints on the Cenozoic, OIB-type alkaline volcanic rocks of NW Turkey: Implications for mantle sources and melting processes. *Lithos*, 86, 50–76.
 Alifirova, T.A., Pokhilenko, L.N., Ovchinnikov, Y.I., Donnelly, C.L., Riches, A.J.V., and Taylor, L.A. (2012) Petrologic origin of exsolution textures in mantle minerals: evidence in pyroxenitic xenoliths from Yakutia kimberlites. *International Geology Review*, 54, 1071–1092.
 Angel, R.J. (1997) Transformation of fivefold-coordinated silicon to octahedral silicon in calcium silicate, $CaSi_2O_5$. *American Mineralogist*, 82, 836–839.
 Angel, R.J., Ross, N.L., Seifert, F., and Fliervoet, T.F. (1996) Structural characterization of pentacoordinate silicon in a calcium silicate. *Nature*, 384, 441–444.
 Angel, R.J., Kunz, M., Miletich, R., Woodland, A.B., Koch, M., and Knoche, R.L. (1999) Effect of isovalent Si,Ti substitution on the bulk moduli of $Ca(Ti_{1-x}Si_x)SiO_3$ titanites. *American Mineralogist*, 84, 282–287.
 Backhaus-Ricoult, M., Mozdziarz, N., and Eveno, P. (1993) Impurities in silicon carbide ceramics and their role during high-temperature creep. *Journal de Physique III*, 3, 2189–2210.
 Bai, W., Zhou, M., and Robinson, P.T. (1993) Possibly diamond-bearing mantle peridotites and podiform chromitites in the Luobusa and Donqiao ophiolites, Tibet. *Canadian Journal of Earth Sciences*, 30, 1650–1659.
 Bai, W., Robinson, P.T., Fang, Q., Yang, J., Yan, B., Zhang, Z., Hu, X., Zhou, M., and Malpas, J. (2000) The PGE and base-metal alloys in the podiform chromitites of the Luobusa ophiolite, southern Tibet. *Canadian Mineralogist*, 38, 585–598.
 Bai, W., Yang, J., Fang, Q., Yan, B., and Shi, R. (2003) An unusual mantle mineral group in ophiolites of Tibet. *Geology in China*, 30, 144–150.
 Barkley, M.C., Downs, R.T., and Yang, H. (2011) Structure of walsstromite, $BaCa_2Si_2O_9$, and its relationship to $CaSiO_3$ -walsstromite and wollastonite-II. *American Mineralogist*, 96, 797–801.
 Bauer, J., Fiala, J., and Hrichová, R. (1963) Natural α -silicon carbide. *American Mineralogist*, 48, 620–634.
 Beck, P., Gillet, P., Gautron, L., Daniel, I., and El Goresy, A. (2004) A new natural high-pressure (Na,Ca)-hexaluminosilicate $[(Ca_xNa_{1-x})Al_{3+x}Si_{3-x}O_{11}]$ in shocked Martian meteorites. *Earth and Planetary Science Letters*, 219, 1–12.
 Bläss, U.W., Langenhorst, F., Frost, D.J., and Seifert, F. (2007) Oxygen deficient perovskites in the system $CaSiO_3$ - $CaAlO_2$ and implications for the Earth's interior. *Physics and Chemistry of Minerals*, 34, 363–376.
 Bouhifd, M.A., Gruener, G., Mysen, B.O., and Richet, P. (2002) Premelting and calcium mobility in gehlenite ($Ca_2Al_2Si_2O_7$) and pseudowollastonite ($CaSiO_3$). *Physics and Chemistry of Minerals*, 29, 655–662.
 Boyko, E.R., and Wisnyski, L.G. (1958) The optical properties and structures of $CaO \cdot 2Al_2O_3$ and $SrO \cdot 2Al_2O_3$. *Acta Crystallographica*, A11, 444–445.
 Brearley, A.J., and Jones, R.H. (1998) Chondritic meteorites. In P.H. Ribbe, Ed., *Planetary Materials*, 36, 3–1–3–398. Reviews in Mineralogy, Mineralogical Society of America, Chantilly, Virginia.
 Brenker, F.E., Vincze, L., Vekemans, B., Nasdala, L., Stachel, T., Vollmer, C., Kersten, M., Somogyi, A., Adams, F., Joswig, W., and Harris, J.W. (2005) Detection of a Ca-rich lithology in the earth's deep (>300 km) convecting mantle. *Earth and Planetary Science Letters*, 236, 579–587.
 Daniel, I., Gillet, P., McMillan, P.F., and Richet, P. (1995) An in situ high-temperature structural study of stable and metastable $CaAl_2Si_2O_9$ polymorphs. *Mineralogical Magazine*, 59, 25–33.
 Daulton, T.L., Bernatowicz, T.J., Lewis, R.S., Messenger, S., Stadermann, F.J., and Amari, S. (2002) Polytopy distribution in circumstellar silicon carbide. *Science*, 296, 1852–1855.
 De, S., Heaney, P.J., Hargraves, R.B., Vincenzi, E.P., and Taylor, P.T. (1998) Microstructural observations of polycrystalline diamond: a contribution to the carbonado conundrum. *Earth and Planetary Science Letters*, 164, 421–433.
 Di Pierro, S., Gnos, E., Grobety, B.H., Armbruster, T., Bemasconi, S.M., and Ulmer, P. (2003) Rock-forming moissanite (natural α -silicon carbide). *American Mineralogist*, 88, 1817–1821.
 Dobrzynetskaia, L., and Green, H.W. (2007) Diamond synthesis from graphite in the presence of water and SiO_2 : Implications for diamond formation in quartzites from Kazakhstan. *International Geology Review*, 49, 389–400.
 Dörsam, G., Liebscher, A., Wunder, B., Franz, G., and Gottschalk, M. (2009) Crystal structure refinement of synthetic $Ca_{0.43}Sr_{0.57}[SiO_3]$ -walsstromite and walsstromite-fluid Ca-Sr distribution at upper-mantle conditions. *European Journal of Mineralogy*, 21, 705–714.
 Essene, E.J., and Fisher, D.C. (1986) Lightning strike fusion: extreme reduction and metal-silicate liquid immiscibility. *Science*, 234, 189–193.
 Gao, C., and Liu, Y. (2008) Moissanite-bearing carbonatite xenoliths from Cenozoic basalt, North China: Products of ancient oceanic crust subduction? *Geochimica et Cosmochimica Acta*, 72(12), A292.
 Gasparik, T., Wolf, K., and Smith, C.M. (1994) Experimental determination of phase relations in the $CaSiO_3$ system from 8 to 15 GPa. *American Mineralogist*, 79,

- 1219–1222.
- Gauthier, J.P. (1978) Polytypisme du carbure de silicium: intérêt de la diffraction électronique par réflexion, 161p. Ph.D thesis, Université Claude-Bernard, France.
- Gautron, L., and Madon, M. (1994) A study of the stability of anorthite in the PT conditions of Earth's transition zone. *Earth and Planetary Science Letters*, 125, 281–291.
- Gautron, L., Angel, R.J., and Mileitch, R. (1999) Structural characterization of the high-pressure phase $\text{CaAl}_2\text{Si}_2\text{O}_{11}$. *Physics and Chemistry of Minerals*, 27, 47–51.
- Golovko, A.V., and Kaminsky, F. (2010) The Shoshonite-Absarokite-Picrite Karashoho Pipe, Uzbekistan: An unusual diamond deposit in an atypical tectonic environment. *Economic Geology*, 105, 825–840.
- Grady, M.M., Verchovsky, A.B., and Wright, I.P. (2004) Magmatic carbon in Martian meteorites: attempts to constrain the carbon cycle on Mars. *International Journal of Astrobiology*, 3, 117–124.
- Gray, I.E., Madsen, I.C., Hibberson, W.O., and O'Neill, H.St.C. (2000) $\text{CaAl}_{12}\text{Si}_4\text{O}_{27}$, a new high-pressure phase containing Al_6O_{19} clusters. *Journal of Solid State Chemistry*, 153, 391–397.
- Gréaux, S., Gautron, L., Andraut, D., Bolfan-Casanova, N., Guignot, N., and Bouhifd, M.A. (2009) Experimental high pressure and high temperature study of the incorporation of uranium in Al-rich CaSiO_3 perovskite. *Physics of the Earth and Planetary Interiors*, 174, 254–263.
- Gréaux, S., Nishiyama, N., Kono, Y., Gautron, L., Ohfuji, H., Kunimoto, T., Menguy, N., and Irifune, T. (2011a) Phase transformations of $\text{Ca}_3\text{Al}_2\text{Si}_3\text{O}_{12}$ grossular garnet to the depths of the Earth's mantle transition zone. *Physics of the Earth and Planetary Interiors*, 185, 89–99.
- Gréaux, S., Nishiyama, N., Kono, Y., Irifune, T., and Gautron, L. (2011b) P-V-T equation of state of $\text{CaAl}_2\text{Si}_2\text{O}_{11}$ CAS phase. *Physics and Chemistry of Minerals*, 38, 581–590.
- Gréaux, S., Farges, F., Gautron, L., Trcera, N., Flank, A.M., and Lagarde, P. (2012) X-ray absorption near edge structure (XANES) study of the speciation of uranium and thorium in Al-rich CaSiO_3 perovskite. *American Mineralogist*, 96, 100–109.
- Hazen, R.M., Papineau, D., Bleeker, W., Downs, R.T., Ferry, J., McCoy, T., Sverjensky, D., and Yang, H. (2008) Mineral evolution. *American Mineralogist*, 93, 1693–1720.
- Hazen, R.M., Downs, R.T., Jones, A.P., and Kah, L. (2013) Carbon mineralogy and crystal chemistry. *Reviews in Mineralogy and Geochemistry*, 75, 7–46.
- Hin, R.C., Fitoussi, C., Schmidt, M.W., and Bourdon, B. (2014) Experimental determination of the Si isotope fractionation factor between liquid metal and liquid silicate. *Earth and Planetary Science Letters*, 387, 55–66.
- Hirose, K., Fei, Y., Ma, Y., and Mao, H.K. (1999) The fate of subducted basaltic crust in the Earth's lower mantle. *Nature*, 397, 53–56.
- Hofmeister, A.M., Wopenka, B., and Locoock, A.J. (2004) Spectroscopy and structure of hibonite, grossite and CaAl_2O_4 : Implications for astronomical environments. *Geochimica et Cosmochimica Acta*, 68, 4485–4503.
- Horita, J., and Polyakov, V.B. (2015) Carbon-bearing iron phases and the carbon isotope composition of the deep Earth. *Proceedings of the National Academy of Sciences*, 112, pp. 31–36.
- Hough, R.M., Gilmour, I., Pillinger, C.T., Arden, J.W., Gilkes, K.W.R., Yuan, J., and Milledge, H.J. (1995) Diamond and silicon carbide in impact melt rock from the Ries impact crater. *Nature*, 378, 41–44.
- Innocenti, F., Agostini, S., Di Vincenzo, G., Doglioni, C., Manetti, P., Savaşçin, M.Y., and Tonerari, S. (2005) Neogene and Quaternary volcanism in Western Anatolia: Magma sources and geodynamic evolution. *Marine Geology*, 221, 397–421.
- Irifune, T., Ringwood, A.E., and Hibberson, W.O. (1994) Subduction of continental crust and terrigenous and pelagic sediments: an experimental study. *Earth and Planetary Science Letters*, 126, 351–368.
- Ishibashi, K., Hirose, K., Sata, N., and Ohishi, Y. (2008) Dissociation of CAS phase in the uppermost lower mantle. *Physics and Chemistry of Minerals*, 35, 197–200.
- Jambor, J.L., and Vanko, D.A. (1992) New mineral names. *American Mineralogist*, 77, 446–452.
- Jaques, A.L., Hall, A.E., Sheraton, J.W., Smith, C.B., Sun, S.S., Drew, R.M., Foudoulis, C., and Ellingsen, K. (1989) Composition of crystalline inclusions and C-isotopic composition of Argyle and Ellendale diamonds. In J. Ross, Ed., *Proceedings of the Fourth International Kimberlite Conference, Kimberlite and Related Rocks, Volume 2: Their Mantle/Crust Setting, Diamonds and Diamond Exploration*. Geological Society of Australia Special Publication 14, p. 966–989. Blackwell Scientific, Cambridge, U.K.
- Jepps, N.W., and Page, T.F. (1983) Polytropic transformations in silicon carbide. In P. Krishna, Ed., *Crystal Growth and Characterization of Polytype Structures*, 7, 259–307. Pergamon Press, Oxford, U.K.
- Joswig, W., Stachel, T., Harris, J.W., Baur, W.H., and Brey, G.P. (1999) New Ca-silicate inclusions in diamonds—tracers from the lower mantle. *Earth and Planetary Science Letters*, 173, 1–6.
- Joswig, W., Paulus, E.F., Winkler, B., and Milman, V. (2003) The crystal structure of CaSiO_3 -walsstromite, a special isomorph of wollastonite-II. *Zeitschrift für Kristallographie*, 218, 811–818.
- Kaminsky, F. (2012) Mineralogy of the lower mantle: A review of 'super-deep' mineral inclusions in diamond. *Earth-Sciences Reviews*, 110, 127–147.
- Kanzaki, M., Stebbins, J.F., and Xue, X. (1998) Characterization of quenched high pressure phases in CaSiO_3 system by XRD and ^{29}Si NMR. *Geophysical Research Letters*, 18, 463–466.
- Kawai, K., and Tsuchiya, T. (2012) First principles investigations on the elasticity and phase stability of grossular garnet. *Journal of Geophysical Research B: Solid Earth*, 117, B02202.
- Kimura, M., Mikouchi, T., Suzuki, A., Miyahara, M., Ohtani, E., and El Goresy, A. (2009) Kushiroite, CaAlAlSiO_6 : A new mineral of the pyroxene group from the ALH 85085 CH chondrite, and its genetic significance in refractory inclusions. *American Mineralogist*, 94, 1479–1482.
- Klein-BenDavid, O., Wirth, R., and Navon, O. (2007) Micrometer-scale cavities in fibrous and cloudy diamonds—A glance into diamond dissolution events. *Earth and Planetary Science Letters*, 264, 89–103.
- Knippenberg, W.F. (1963) Growth phenomena in silicon carbide. *Philips Research Reports*, 18, 161–274.
- Komabayashi, T., Hirose, K., Sata, N., Ohishi, Y., and Dubrovinsky, L.S. (2007) Phase transition in CaSiO_3 perovskite. *Earth and Planetary Science Letters*, 260, 564–569.
- Kojitani, H., Wakabayashi, Y., Tejima, Y., Kato, C., Haraguchi, M., and Akaogi, M. (2009) High-pressure phase relations in $\text{Ca}_2\text{AlSiO}_{5.5}$ and energetics of perovskite-related compounds with oxygen defects in the $\text{Ca}_2\text{Si}_2\text{O}_6$ - $\text{Ca}_2\text{Al}_2\text{O}_3$ join. *Physics of the Earth and Planetary Interiors*, 173, 349–353.
- Krot, A., Fagan, T.J., Keil, K., McKeegan, K.D., Sahjpal, S., Hutcheon, I.D., Petaev, M.I., and Yurimoto, H. (2004) Ca, Al-rich inclusions, amoeboid olivine aggregates, and Al-rich chondrules from the unique carbonaceous chondrite Acfer 094: I. Mineralogy and petrology. *Geochimica et Cosmochimica Acta*, 68, 2167–2184.
- Kudoh, Y., and Kanzaki, M. (1998) Crystal chemical characteristics of α - CaSi_2O_5 , a new high pressure calcium silicate with five-coordinated silicon synthesized at 1500 °C and 10 GPa. *Physics and Chemistry of Minerals*, 25, 429–433.
- Kurashina, T., Hirose, K., Ono, S., Sata, N., and Ohishi, Y. (2004) Phase transition in Al-bearing CaSiO_3 perovskite: implications for seismic discontinuities in the lower mantle. *Physics of the Earth and Planetary Interiors*, 145, 67–74.
- Leung, I.S. and Kuo, W.X. (1988) Abundant moissanite found in Fuxian diamond pipe, Liaoning, China. Geological Society of America 1988 Centennial Celebration, Denver, Colorado, Oct. 31–Nov. 3, 1988 Conference Proceeding, Abstract 20850.
- (1990) Silicon carbide cluster entrapped in a diamond from Fuxian, China. *American Mineralogist*, 75, 1110–1119.
- Leung, I.S., Guo, W., Friedman, I., and Gleason, J. (1990) Natural occurrence of silicon carbide in a diamondiferous kimberlite from Fuxian. *Nature*, 346, 352–354.
- Leung, I.S., Taylor, L.A., Tsao, C.S., and Han, Z. (1996) SiC in diamond and kimberlites: Implications for nucleation and growth of diamond. *International Geology Review*, 38, 595–606.
- Liang, F., Xu, Z., and Zhao, J. (2014) In situ moissanite in dunite: Deep mantle origin of mantle peridotite in Luobusa ophiolite, Tibet. *Acta Geologica Sinica (English ed.)*, 88, 517–529.
- Lindstad, L.H. (2002) Recrystallization of silicon carbide. Thesis/Dissertation, Department of Materials Technology and Electrochemistry Norwegian University of Science and Technology N-7491 Trondheim.
- Liu, X., Wang, S., He, Q., Chen, J., Wang, H., Li, S., Peng, F., Zhang, L., and Fei, Y. (2012) Thermal elastic behavior of CaSiO_3 -walsstromite: A powder X-ray diffraction study up to 900 °C. *American Mineralogist*, 97, 262–267.
- Ma, C., Simon, S.B., Rossman, G.R., and Grossman, L. (2009) Calcium Tschermak's pyroxene, CaAlAlSiO_6 , from the Allende and Murray meteorites: EBSD and micro-Raman characterizations. *American Mineralogist*, 94, 1483–1486.
- Ma, C., Krot, A.N., and Bizzarro, M. (2013) Discovery of dmisterbergite (hexagonal $\text{CaAl}_2\text{Si}_2\text{O}_6$) in the Allende meteorite: A new member of refractory silicates formed in the solar nebula. *American Mineralogist*, 98, 1368–1371.
- Mao, H., Hillert, M., Sellby, M., and Sundman, B. (2006) Thermodynamic assessment of the $\text{CaO-Al}_2\text{O}_3$ - SiO_2 system. *Journal of the American Ceramic Society*, 89, 298–308.
- Marakushev, A.A., Glazovskaya, L.I., and Marakushev, S.A. (2013) Evolution of the iron-silicate and carbon material of carbonaceous chondrites. *Moscow University Geology Bulletin*, 68, 265–281.
- Marshintsev, V.K. (1990) Nature of silicon carbide in kimberlites rocks of Yakutia. *Mineralogicheskiy Zhurnal*, 12, 17–26.
- Mathez, E.A., Fogel, R.A., Hutcheon, I.D., and Marshintsev, V.K. (1995) Carbon isotopic composition and origin of SiC from kimberlites of Yakutia, Russia. *Geochimica et Cosmochimica Acta*, 59, 781–791.
- McCammon, C., Hutchinson, M., and Harris, J.W. (1997) Ferric iron content of mineral inclusions in diamonds from São Luiz: A view into the Lower Mantle. *Science*, 278, 434–436.
- Milton, C., and Vitaliano, D.B. (1984) The non-existence of moissanite, SiC. 27th International Geological Congress, 5, 107–108.
- Moissan, H. (1905) Etude du silicure de carbone de la météorite de Cañon Diablo. *Comptes-rendus Académie des Sciences (Paris)*, 140, 405–406.
- Moore, R.O., and Gurney, J.J. (1989) Mineral inclusions in diamond from the Monastery kimberlite, South Africa. In J. Ross, Ed., *Proceedings of the Fourth International Kimberlite Conference, Kimberlite and Related Rocks, Volume 2: Their Mantle/Crust Setting, Diamonds and Diamond Exploration*. Geological Society of Australia Special Publication 14, p. 1029–1041. Blackwell Scientific, Cambridge, U.K.
- Moore, R.O., Otter, M.L., Rickard, R.S., Harris, J.W., and Gurney, J.J. (1986) The occurrence of moissanite and ferro-periclaase as inclusions in diamond. In 4th In-

- ternational Kimberlite Conference, Perth, Extended Abstracts; Abstract Geological Society of Australia, 16, 409–411.
- More, K.L., Carter, C.H., Bentley, J., Wadlin, W.H., Lavanier, L., and Davis, R.F. (1986) Occurrence and distribution of Boron-containing phases in sintered α -silicon carbide. *Journal of the American Ceramic Society*, 69, 695–698.
- Munro, R.G. (1997) Material properties of a sintered α -SiC. *Journal of Physical and Chemical Reference Data*, 26, 1195–1203.
- Nasdala, L., Brenker, F. E., Glinemann, J., Hofmeister, W., Gasparik, T., Harris, J. W., Stachel, T., and Reese, I. (2003) Spectroscopic 2D-tomography: Residual pressure and strain around mineral inclusions in diamonds. *European Journal of Mineralogy*, 15, 931–935.
- Nestola, F., Mitterperger, S., Di Toro, G., Zorzi, F., and Pedron, D. (2010) Evidence of dmisteinbergite (hexagonal form of $\text{CaAl}_2\text{Si}_2\text{O}_8$) in pseudotachylyte: A tool to constrain the thermal history of a seismic event. *American Mineralogist*, 95, 405–409.
- Nishi, M., Kubo, T., Kato, T., Tominaga, A., Funakoshi, K.I., and Higo, Y. (2011) Exsolution kinetics of majoritic garnet from clinopyroxene in subducting oceanic crust. *Physics of the Earth and Planetary Interiors*, 189, 47–55.
- Nomura, K., and Miyamoto, M. (1998) Hydrothermal experiments on alteration of Ca-Al-rich inclusions (CAls) in carbonaceous chondrites: Implication for aqueous alteration in parent asteroids. *Geochimica et Cosmochimica Acta*, 62, 3575–3588.
- Okamura, F.P., Ghose, S., and Ohashi, H. (1974) Structure and crystal chemistry of Calcium Tschermak's pyroxene, CaAlAlSiO_6 . *American Mineralogist* 59, 549–557.
- Oleynikov, B.V., Pankov, V.Y., Plaksenko, A.N., and Okrugin, A.V. (1987) Inclusions in moissanite from mafic rocks of cratons. *Transactions (Doklady) of the U.S.S.R. Academy of Sciences: Earth Science Sections*, 283, 155–159.
- Osborn, E.F., and Muan, A. (1960) Phase equilibrium diagrams of oxide systems. Plate 2. The system $\text{CaO-Al}_2\text{O}_3\text{-SiO}_2$. American Ceramic Society, Columbus, Ohio.
- Otter, M.L., and Gurney, J.J. (1986) Mineral inclusions in diamonds from the Sloan diatremes. Colorado-Wyoming State Line Kimberlite District, North America In 4th International Kimberlite Conference, Perth, Extended Abstracts; Abstract Geological Society of Australia, 16, 415–417.
- (1989) Mineral inclusions in diamonds from the Sloan diatremes, Colorado-Wyoming State Line kimberlite district, North America. In J. Ross, Ed., *Proceedings of the Fourth International Kimberlite Conference, Kimberlite and Related Rocks, Volume 2: Their Mantle/Crust Setting, Diamonds and Diamond Exploration*. Geological Society of Australia Special Publication 14, p. 1042–1053. Blackwell Scientific, Cambridge, U.K.
- Pankov, V.Y., and Spetsius, Z.V. (1990) Iron silicide and native silicon inclusions in moissanite from the Sytykan kimberlite pipe. *Transactions (Doklady) of the U.S.S.R. Academy of Sciences Earth Science Sections*, 305, 152–155.
- Perraki, M., and Faryad, S.W. (2014) First finding of microdiamond, coesite and other UHP phases in felsic granulites in the Moldanubian Zone: Implications for deep subduction and a revised geodynamic model for Variscan Orogeny in the Bohemian Massif. *Lithos*, 202–203, 157–166.
- Qi, X.X., Yang, J.S., Xu, Z.Q., Bai, W.J., Zhang, Z.M., and Fang, Q.S. (2007) Discovery of moissanite in retrogressive eclogite from the Pre-pilot Hole of the Chinese Continental Scientific Drilling Project (CCSD-PP2) and its geological implication. *Acta Petrologica Sinica*, 23, 3207–3214.
- Robinson, P.T., Bai, W.J., Malpas, J., Yang, J.S., Zhou, M.F., Fang, Q.S., Hu, X.F., Cameron, S., and Staudigel, H. (2004) Ultra-high pressure minerals in the Loubusa Ophiolite, Tibet, and their tectonic implications. *Geological Society of London, Special Publications*, 226, 247–271.
- Robinson, P.T., Trumbull, R.B., Schmitt, A., Yang, J.S., Li, J.W., Zhou, M.F., Erzinger, J., Dare, S., and Xiong, F. (2015) The origin and significance of crustal minerals in ophiolitic chromitites and peridotites. *Gondwana Research*, 27, 486–506.
- Sameshima, T., and Rodgers, K.A. (1990) Crystallography of 6H silicon carbide from Seddonville, New Zealand. *Neues Jahrbuch für Mineralogie Monatshefte*, 3, 137–143.
- Schmidt, M.W., Gao, C., Golubkova, A., Rohrbach, A., and Connolly, J.A.D. (2014) Natural moissanite (SiC)—a low temperature mineral formed from highly fractionated ultra-reducing COH-fluids. *Progress in Earth and Planetary Science*, 1, 1–14.
- Schoenitz, M., Navrotsky, A., and Ross, N. (2001) Enthalpy of formation of CaSi_2O_6 : a quenched high-pressure phase with pentacoordinate silicon. *Physics and Chemistry of Minerals*, 28, 57–60.
- Seryotkin, Y.V., Sokol, E.V., and Kokh, S.N. (2012) Natural pseudowollastonite: Crystal structure, associated minerals, and geological context. *Lithos*, 134–135, 75–90.
- Sharma, S.K., Simons, B., and Yoder, H.S. (1983) Raman study of anorthite, calcium Tschermak's pyroxene and gehlenite in crystalline and glassy states. *American Mineralogist*, 68, 1113–1125.
- Shim, S., Duffy, T.S., and Shen, G. (2000) The stability and P-V-T equation of state of CaSiO_3 perovskite in the Earth's lower mantle. *Journal of Geophysical Research*, 105, 25955–25968.
- Shiryaev, A.A., and Gaillard, F. (2014) Local redox buffering by carbon at low pressures and the formation of moissanite—natural SiC. *European Journal of Mineralogy*, 26, 53–59.
- Shiryaev, A.A., Griffin, W.L., and Stoyanov, E. (2011) Moissanite (SiC) from kimberlites: Polytypes, trace elements, inclusions and speculations on origin. *Lithos*, 122, 152–164.
- Shirey, S.B., Cartigny, P., Frost, D.J., Keshav, S., Nestola, F., Nimis, P., Pearson, D.G., Sobolev, N.V., and Walter, M.J. (2013) Diamonds and the Geology of Mantle Carbon. *Reviews in Mineralogy and Geochemistry*, 75, 355–421.
- Simon, S.B., and Grossman, L. (2011) Refractory inclusions in the unique carbonaceous chondrite Acfer 094. *Meteoritics and Planetary Science*, 46, 1197–1216.
- Sokol, E., Volkova, N., and Lepezin, G. (1998) Mineralogy of pyrometamorphic rocks associated with naturally burned coal-bearing spoil-heaps of the Chelyabinsk coal basin, Russia. *European Journal of Mineralogy*, 10, 1003–1014.
- Stachel, T. (2001) Diamonds from the asthenosphere and the transition zone. *European Journal of Mineralogy*, 13, 883–892.
- Stebbins, J.F., and Poe, B.T. (1999) Pentacoordinate silicon in high-pressure crystalline and glassy phases of calcium disilicate (CaSi_2O_6). *Geophysical Research Letters*, 26, 2521–2523.
- Sueda, Y., Irifune, T., Yamada, A., Inoue, T., Liu, X., and Funakoshi, K.I. (2006) The phase boundary between CaSiO_3 perovskite and $\text{Ca}_2\text{SiO}_4 + \text{CaSi}_2\text{O}_6$ determined by in situ X-ray observations. *Geophysical Research Letters*, 33, L10307.
- Surkov, N.V., and Doroshev, A.M. (1998) Phase diagram of $\text{CaO-Al}_2\text{O}_3\text{-SiO}_2$ system at pressures of up to 40 kbar. *Russian Geology and Geophysics*, 39, 1257–1272.
- Svisero, D.P. (1995) Distribution and origin of diamonds in Brazil: an overview. *Journal of Geodynamics*, 20, 493–514.
- Swamy, V., and Dubrovinsky, L.S. (1997) Thermodynamic data for the phases in the CaSiO_3 system. *Geochimica et Cosmochimica Acta*, 61, 1181–1191.
- Takafuji, N., Yagi, T., Miyajima, N., and Sumita, T. (2002) Study on Al_2O_3 content and phase stability of aluminous- CaSiO_3 perovskite at high pressure and temperature. *Physics and Chemistry of Minerals*, 29, 532–537.
- Takahashi, S., Ohtani, E., Terasaki, H., Ito, Y., Shibasaki, Y., Ishii, M., Funakoshi, K., and Higo, Y. (2013) Phase relations in the carbon-saturated C-Mg-Fe-Si-O system and C and Si solubility in liquid Fe at high pressure and temperature: implications for planetary interiors. *Physics and Chemistry of Minerals*, 40, 647–657.
- Trumbull, R.B., Yang, J.S., Robinson, P.T., Di Pierro, S., Vennemann, T., and Wiedenbeck, M. (2009) The carbon isotope composition of natural SiC (moissanite) from the Earth's mantle: New discoveries from ophiolites. *Lithos*, 113, 612–620.
- Ulmer, G.C., Grandstaff, D.E., Woermann, E., Göbbles, M., Schönitz, M., and Woodland, A.B. (1998) The redox stability of moissanite (SiC) compared with metal-metal oxide buffers at 1773 K and at pressures up to 90 kbar. *Neues Jahrbuch für Mineralogie Abhandlungen*, 172, 279–307.
- Vanderah, T.A., Loezos, J.M., and Roth, R.S. (1996) Magnetic dielectric oxides: subsolidus phase relations in the $\text{BaO:Fe}_2\text{O}_3\text{:TiO}_2$ system. *Journal of Solid State Chemistry*, 121, 38–50.
- Wang, Y., and Weidner, D.J. (1994) Thermoelasticity of CaSiO_3 perovskite and implications for the Lower Mantle. *Geophysical Research Letters*, 21, 895–898.
- Wang, W., Gasparik, T., and Rapp, R.P. (2000) Partitioning of rare earth elements between CaSiO_3 perovskite and coexisting phases: Constraints on the formation of CaSiO_3 inclusions in diamonds. *Earth and Planetary Science Letters*, 181, 291–300.
- Weber, D., and Bischoff, A. (1994) Grossite (CaAl_2O_6)—a rare phase in terrestrial rocks and meteorites. *European Journal of Mineralogy*, 6, 591–594.
- Wilding, M.C., Harte, B., and Harris, J.W. (1991) Evidence for a deep origin for São Luiz diamonds. *Extended Abstracts 5th International Kimberlite Conference, CPRM Special Publication 2/91*, 456–458.
- Xu, S., Wu, W., Xiao, W., Yang, J., Chen, J., Ji, S., and Liu, Y. (2008) Moissanite in serpentinite from the Dabie Mountains in China. *Mineralogical Magazine*, 72, 899–908.
- Yamamoto, S., Komiya, T., Hirose, K., and Maruyama, S. (2009) Coesite and clinopyroxene exsolution lamellae in chromitites: In situ ultrahigh-pressure evidence from podiform chromitites in the Luobusa ophiolite, southern Tibet. *Lithos*, 109, 314–322.
- Yang, J.S., Xu, X.Z., Li, Y., Li, J.Y., Ba, D.Z., Rong, H., and Zhang, Z.M. (2011) Diamonds recovered from peridotite of the Purang ophiolite in the Yarlung-Zangbo suture of Tibet: A proposal for a new type of diamond occurrence. *Acta Petrologica Sinica*, 27, 3171–3178.
- Yang, J.S., Robinson, P.T., and Dilek, Y. (2014) Diamonds in ophiolites. *Elements*, 10, 127–130.
- Yusa, H., Yagi, T., and Shimobayashi, N. (1995) A new unquenchable high-pressure polymorph of $\text{Ca}_2\text{Al}_2\text{Si}_2\text{O}_{12}$. *Physics of the Earth and Planetary Interiors*, 92, 25–31.
- Zhang, A., and Hsu, W. (2009) Refractory inclusions and aluminum-rich chondrules in Sayh al Uhaymir 290 CH chondrite: Petrography and mineralogy. *Meteoritics and Planetary Science*, 44, 787–804.
- Zhai, S., and Ito, E. (2008) Phase relations of $\text{CaAl}_2\text{Si}_2\text{O}_{11}$ at high-pressure and high-temperature with implications for subducted continental crust into the deep mantle. *Physics of the Earth and Planetary Interiors*, 167, 161–167.
- Zhou, L.Y., and Telle, R. (2010) Purifying mechanism in the achesson process—A thermodynamic study. *Materials Science Forum*, 645–648, 41–44.